Research Article Vol. 3, No. 12 / December 2016 / Optica 1483

Ultralinear heterogeneously integrated ring-assisted Mach–Zehnder interferometer modulator on silicon

Chong Zhang,[1,*] Paul A. Morton,[2] Jacob B. Khurgin,[3] Jon D. Peters,[1] and John E. Bowers[1]

[1]Department of Electrical & Computer Engineering, University of California, Santa Barbara, California 93106, USA
[2]Morton Photonics, West Friendship, Maryland 21794, USA
[3]Department of Electrical and Computer Engineering, Johns Hopkins University, Baltimore, Maryland 21218, USA
*Corresponding author: czhang@ece.ucsb.edu

Received 4 October 2016; revised 14 November 2016; accepted 15 November 2016 (Doc. ID 277992); published 8 December 2016

A linear modulator is indispensable for radio frequency photonics or analog photonic link applications where high dynamic range is required. There is also great interest to integrate the modulator with other photonic components, to create a photonic integrated circuit for these applications, with particular focus on silicon photonics integration in order to take advantage of complementary metal–oxide–semiconductor compatible foundries for high-volume, low-cost devices. However, all silicon modulators, including the highest performing Mach–Zehnder interferometer (MZI) type, have poor linearity, partially due to the inherent nonlinearity of the MZI transfer characteristic, but mostly due to the nonlinearity of silicon's electro-optic phase shift response. In this work, we demonstrate ultralinear ring-assisted MZI (RAMZI) modulators, incorporating heterogeneously integrated III–V multiple quantum wells on silicon phase modulation sections to eliminate the nonlinear silicon phase modulation response. The heterogeneously integrated III–V/Si RAMZI modulators achieve record-high spurious free dynamic range (SFDR) for silicon-based modulators, as high as 117.5 dB · $Hz^{2/3}$ at 10 GHz for a weakly coupled ring design, and 117 dB · $Hz^{2/3}$ for a strongly coupled ring design with higher output power. This is a higher SFDR than typically obtained with commercial lithium niobate modulators. This approach advances integrated modulator designs on silicon for applications in compact and high-performance analog optical systems.

OCIS codes: (130.4110) Modulators; (060.5625) Radio frequency photonics; (230.4205) Multiple quantum well (MQW) modulators.

https://doi.org/10.1364/OPTICA.3.001483

1. INTRODUCTION

A highly linear optical modulator is a key component in radio frequency (RF) photonic and analog fiber optic links and systems, to reduce signal distortion and achieve a high dynamic range [1,2]. Furthermore, an integrated ultralinear modulator on chip is strongly desired in compact, complex analog photonic integrated circuit (PIC) designs [3,4], with requirements well beyond the performance of commonly used silicon-based on-chip modulators. Silicon Mach–Zehnder interferometer (MZI) modulators have shown significantly worse linearity than the lithium niobate ($LiNbO_3$) MZI modulators used in RF photonics systems [5,6]. The best published result for an all-Si MZI modulator shows a 97 dB · $Hz^{2/3}$ spurious free dynamic range (SFDR) at a 1 GHz modulation frequency [7], while a typical optical link using a $LiNbO_3$ MZI modulator may have an SFDR as high as 113 dB · $Hz^{2/3}$ [8]. This is mainly because the index modulation in Si is achieved by a relatively weak mechanism, charge injection, which is strongly nonlinear.

To increase SFDR, linearization techniques can be used, typically some kind of electronic predistortion that increases the modulator complexity and power consumption and usually works only over limited bandwidth [9,10]. A simple all-optical linearization technique, free of the above impediments, is the ring-assisted MZI (RAMZI) modulator that was proposed in 2003 [11]. The RAMZI modulator uses the super-linearity of a ring phase modulator (with high coupling to the MZI arms) to balance the sub-linearity (sinusoidal transfer characteristic) of an MZI modulator. All-Si RAMZI modulators showed significant improvement over all-Si MZI modulators, demonstrating an SFDR of 106 dB · $Hz^{2/3}$ at 1 GHz and 99 dB · $Hz^{2/3}$ at 10 GHz [12]. However, because the index change of silicon has a third-order nonlinear term with the same negative sign as the inherent MZI nonlinearity, the combined negative nonlinearity is so high that canceling it with the opposite-signed nonlinearity of the ring is difficult, as relatively low coupling coefficients become necessary, causing an increase in the insertion loss and thus reducing SFDR. The all-Si RAMZI modulator still showed significantly lower linearity than a commercial $LiNbO_3$ modulator.

In order to overcome the nonlinearity from silicon-based phase modulators, heterogeneous integration of materials with the linear electro-optic (EO) effect onto silicon was researched. Chen *et al.*, reported the integration of $LiNbO_3$, which has a strong linear Pockels effect. A silicon ring modulator with an adherently bonded $LiNbO_3$ thin film achieved a SFDR of 98.1 dB ·

$Hz^{2/3}$ at 1 GHz and 87.6 $dB \cdot Hz^{2/3}$ at 10 GHz [13]. Recent work demonstrated an MZI modulator with the integration of InP-based multiple quantum wells (MQWs) [14]. The III–V layers were bonded to silicon and formed phase modulators on both arms of a silicon MZI. The MZI transfer characteristic has a negative third-order term, as does the III–V MQW plasma-like effect of free carriers and the state-blocking phase change effect. The quantum confined Stark effect (QCSE) has a positive third-order term, and strong wavelength dependence, while the Pockels effect is largely linear [15]. The positive nonlinearity of the QCSE phase response can be sufficient to cancel the negative nonlinearities of the plasma and state-blocking effects at specific wavelength and modulator bias. The heterogeneously integrated MZI modulator achieved a high linearity, with SFDR of 112 $dB \cdot Hz^{2/3}$ at 10 GHz [14].

In this work, we further improve the linearity of III–V/Si MZI modulators through the addition of ring phase modulators, using the RAMZI modulator design to linearize the MZI transfer characteristic. Two options for the RAMZI design are fabricated and tested, one with a weak coupling to the rings, and one with a strong coupling to the rings. In both cases, ultralinear operation is achieved, higher than obtainable in the basic MZI design. Heterogeneous III–V/Si RAMZI modulator design, fabrication, and characterization are discussed in detail in this paper.

2. PRINCIPLE, DESIGN, AND FABRICATION

The operating principle of the RAMZI modulator has been described in previous work [11,12] under the assumption that the index modulation itself is perfectly linear, as is the case with the Pockels effect in $LiNbO_3$. In reality, the index modulation of the heterogeneous III–V/Si phase modulator is more complex as it involves inherently quadratic processes in the reverse biased P-I-N junction with band filling, QCSE, and, to a lesser extent, the free carrier effect [14,15]. It is important to note that both band filling and the QCSE effects are resonant phenomena and exhibit strong wavelength dependence.

To create a MZI modulator with an ultralinear transfer characteristic, the extrinsic nonlinearity of the MZI, which transforms index modulation into intensity modulation, should be balanced by the device design. When a standard heterogeneous MZI modulator is used, its extrinsic third-order nonlinearity is negative and rather large [14]. To cancel it with the intrinsic nonlinearity of the index change would require operation at a wavelength close to the bandgap, which increases insertion loss, causing the SFDR to suffer. The results of the heterogeneous MZI modulator have shown an overall nonlinearity similar to that of the MZI response alone [14].

In the RAMZI modulator design, the total extrinsic nonlinearity of the MZI transfer characteristic is reduced, and the level of reduction is determined by the coupling coefficient κ. With the assumption that the phase section inside the ring changes linearly with bias, as κ is reduced from 1 to $\kappa_0 = 0.86$ the inherent negative nonlinearity of the MZI is reduced to 0, and for lower κ values, this nonlinearity changes its sign, becoming positive [11]. The RAMZI design therefore allows for the cancellation of the nonlinearity inherent in the MZI design, by judicious choice of coupling coefficients plus the use of phase modulation sections with zero, low, and/or tunable nonlinearity. This compensation requires additional design complexity and a tuning process, but once the compensation is attained and the parameters assuring the highest SFDR are determined, the arrangement is proven to be quite robust, and record-high SFDR can be repeatedly measured across modulator parameters and different operating wavelengths.

The device is shown schematically in Fig. 1(a). The symmetric interferometer is formed with a 3 dB multimode interference (MMI) coupler and a directional coupler as power splitter and combiner, respectively. Both arms of the MZI couple to a ring/racetrack resonator through a directional coupler with a specific coupling coefficient, κ. In each racetrack, the low-loss silicon ridge waveguide adiabatically transits to two heterogeneous sections through a 50 μm long taper on one side, and on the other

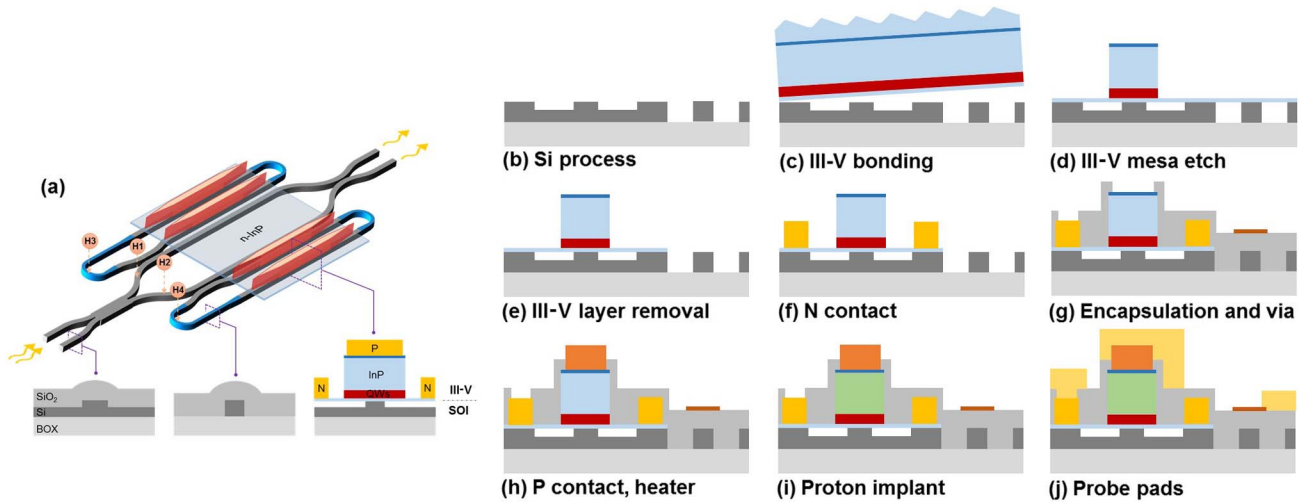

Fig. 1. (a) Schematic structure of heterogeneous RAMZI modulator on silicon with different colors representing ridge/stripe/heterogeneous waveguide and corresponding cross sections. The symmetric architecture includes two rings with heterogeneous phase sections, with H1–H4 indicating the locations of extra thermal phase tuners. (b)–(j) Process flow of the heterogeneous RAMZI modulator: (b) define the passive components on silicon; (c) transfer III–V layers to patterned SOI substrate, and remove the InP substrate through wet-etch; (d) etch the III–V mesa and QWs stack; (e) remove the III–V layer on the waveguide; (f) deposit n-type contact metal stack on n-InP; (g) encapsulate the surface with thick SiO_2 layer and etch deep via; (h) deposit p-type contact metal stack, deposit heater metal stack; (i) proton implant to isolate the taper and modulator cavity; and (j) deposit metal probe pads.

side transits to a fully etched nano-stripe waveguide, required for the tight bending radius of 15 μm. Three types of waveguides, with cross sections shown in Fig. 1(a), form the total ring circumference. Both MZI arms and both rings have a separate heater for phase tuning (H1–H4), to control the device operation point. The two heterogeneous sections in each ring have a 250 μm long and 2.5 μm wide mesa. The silicon waveguide under the III–V mesa is 600 nm in width, to increase the optical mode confinement factor in the III–V MQW stack, which consists of 12 QWs with PL wavelength centered at 1360 nm, as described in the detailed design in [14]. The cathodes of all four active sections are connected as the bias port for push–pull operation [16]. Two types of RAMZI modulator were fabricated: strong- and weak-coupled ring designs, with the as-fabricated power coupling ratio determined to be 0.79 and 0.55, representing the coupling coefficients to be 0.89 and 0.74, respectively.

The heterogeneous RAMZI devices were fabricated in house using the process flow shown in Figs. 1(b)–1(j). First, an SOI wafer with 500 nm device thickness and 1 μm buried oxide layer (BOX) was patterned with a 248 nm deep ultraviolet lithographic tool, and then etched with $C_4F_8/SF_6/Ar$ in a reactive ion etch (RIE) tool. After III–V die bonding onto the SOI wafer and removing the InP substrate, the thin III–V film included the n-InP contact layer, AlGaInAs MQWs stack, p-doped InP cladding, and p-InGaAs contact layer (n-side down). It is worth noting that neither precise position alignment nor high temperature anneal was required for the wafer bonding process. A complementary metal–oxide–semiconductor (CMOS) compatible top-down process was then performed. The 2.5 μm wide mesa was etched with methane/H_2/Ar RIE etch, and then the MQW layer was wet etched to expose the n-contact layer. After the n-type metallization, a thick SiO_2 layer was deposited to protect and isolate the devices. P-type metal was deposited after a deep via was etched on top of the mesa. Pd/Ti/Pd/Au and Pd/Ge/Pd/Au metal stacks were deposited as contact metals for p- and n-type contacts, respectively. Then a Ni/Cr heater layer with total thickness of 100 nm was deposited on top of the Si waveguide. A proton implant was adopted to isolate the mesa with the tapers. Finally, thick metal pads were deposited on both n- and p-contact metal for probe contact. The chip was diced into columns, and the waveguide facet was mechanically polished for fiber coupling. The silicon waveguide is flared out to 5 μm with an 8° angle to reduce the facet reflection. Chips with polished facets were mounted to a heat sink with temperature controlled. The output from a tunable laser source was coupled into the input port with a lensed fiber. At the output port of the modulators, light was coupled back to fiber for performance analysis.

3. RESULTS AND DISCUSSION

A ground–signal–ground (GSG) probe provides the modulation signal for the device, modulating two straight sections of each ring in a push–pull configuration, with the *n* contact providing the DC bias voltage level [3], as shown in Fig. 2. Thermal tuners H1 and H2 are used to tune the MZI phase and set the bias point of the MZI, e.g., at quadrature. Thermal tuners H3 and H4 are used to tune the resonance frequencies of the two rings. A tunable laser was used to characterize the device. High laser output power, 15 or 18 dBm, was coupled into the on-chip modulator; however, due to the high coupling loss between the silicon waveguide and lensed fiber, which was ~9 dB per facet, a lower power level was

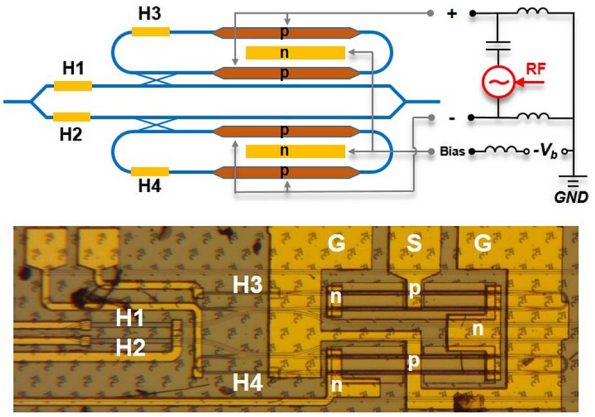

Fig. 2. Heterogeneous RAMZI modulator with push–pull differential configurations and its microscope image.

present within the RAMZI modulator. Alternatively, an amplified spontaneous emission (ASE) source was used to monitor the transmission spectrum through the modulator.

The insertion loss of the strong-coupled RAMZI modulator itself (removing the coupling loss of the two fiber-to-waveguide couplings) was 9 dB, compared to 3.7 dB for the short (100 μm) MZI device in [14], which had only 0.7 dB excess loss as the modulator bias was set to quadrature. This additional loss in the RAMZI is from absorption from the longer active sections, plus the optical loss from the four tapered mode convertors and the passive silicon waveguides. Much lower loss could be achieved in an optimized III–V/Si ring structure. Additional insertion loss is present when varying the bias conditions of the rings. Figure 3 shows the effect of changing each phase tuner in the RAMZI modulator with strong-coupled rings ($\kappa = 0.79$). Figures 3(a) and 3(b) show the effects of MZI phase heaters H1 and H2, respectively. At zero voltage, the black traces in both figures show the unbiased device spectra, with the ring "dips" clear; the device should be biased near the high point between these dips. Increasing bias voltage in H1 moves the MZI phase in one

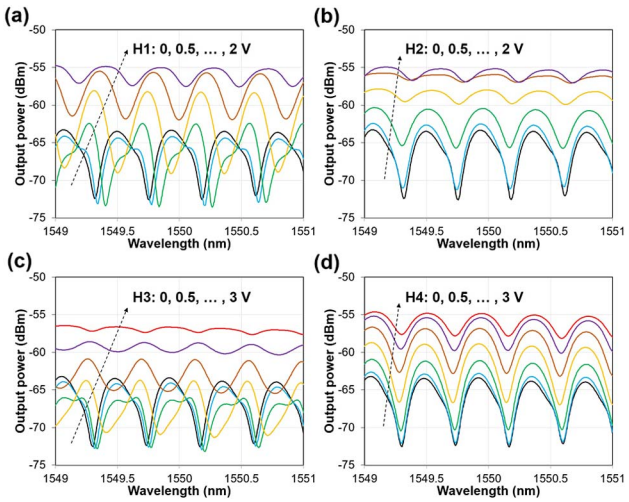

Fig. 3. Transmission spectrum of the heterogeneous RAMZI modulator with strong-coupled rings with ASE input. (a)–(d) show the operation point change by applying voltage on thermal tuners H1–H4, respectively, with all other tuners unbiased.

direction, while in H2, it moves it in the other direction. Increasing the bias voltage in H1, as shown in Fig. 3(a), initially reduces the output power to its minimum level, and then it increases. Increasing the bias voltage in H2, as shown in Fig. 3(b), provides a more symmetrical spectrum for small voltages with a value of 1 V providing a reasonable output power.

Figures 3(c) and 3(d) show spectra changes from tuning the ring resonance heaters H3 and H4. Similar changes are seen in these spectra as for tuning the MZI phase, indicating that the heaters have thermal crosstalk and that in these devices all heaters affect both MZI phase and ring resonance frequency. From Fig. 3 it can be seen that the ring resonance frequencies tune a relatively small amount, much less than one free spectral range (FSR), while the MZI phase is more effectively tuned. This should be taken into account when looking at SFDR results for various heater values, e.g., H2 and H4 having a somewhat similar bias effect on the device.

The modulator linearity was characterized through measurements of SFDR at 1550 nm, for a modulation frequency of 10 GHz. The tunable laser was set at a wavelength midway between a pair of dips in the optical spectrum. The modulator output is amplified in an erbium-doped fiber amplifier (EDFA) to overcome the large coupling losses of the device (18 dB total), followed by a narrow filter to reduce the ASE added by the EDFA. The fundamental and third-order intermodulation products of the modulation were measured using two RF tone input [14]. The modulator's SFDR was measured at different phase modulator bias voltages and heater voltages.

By carefully tuning the thermal phase tuners H1–H4 and the modulator bias voltage, the highest SFDR for the RAMZI with strong-coupled rings was achieved for a modulator bias of –3 V and for H4 = 1.2 V, as shown in Fig. 4; the measurement includes the fundamental and third-order intermodulation products, and noise level for 1 GHz bandwidth (–69 dBm), providing an SFDR of 57 dB for 1 GHz bandwidth, equivalently an SFDR of 117 dB · $Hz^{2/3}$. This is a 5 dB improvement in SFDR compared to a commercial $LiNbO_3$ modulator measured on the same setup. With this strong-coupled device, this high value of SFDR was achieved at the lowest modulator loss, ~9 dB.

Figure 5(a) shows a series of SFDR measurements for the strong-coupled RAMZI modulator as the MZI phase heaters and ring heaters were varied. The SFDR is very high near zero bias, over 115 dB · $Hz^{2/3}$. Varying the MZI phase heaters, H1 and H2 (with H3 and H4 = 0 V), a small maximum is found for H2 = 1 V, providing an SFDR of 116 dB · $Hz^{2/3}$. Varying the ring heaters' voltages, H3 and H4 (with H3 and H4 = 0 V), the maximum SFDR value of 117 dB · $Hz^{2/3}$ is seen for a number of H4 values of 1.2, 1.3, and 1.4 V.

Figure 5(b) shows a series of measured SFDR values versus the modulator DC bias level, for laser input powers of 15 and 18 dBm. At the lower laser power level of 15 dBm, the SFDR peaks near a bias of –2.5 V, whereas at the higher laser power of 18 dBm, the SFDR peak moves down to –3 V.

Both the SFDR and the modulator output power P_{out}, i.e., the internal power before output fiber coupling, vary as the input laser wavelength is varied over more than a full FSR of the ring

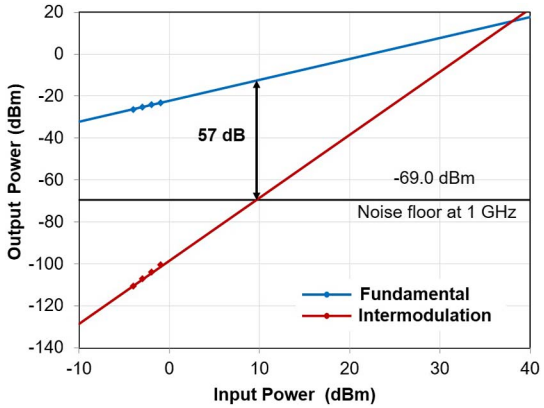

Fig. 4. Measured SFDR of heterogeneous RAMZI modulator with strong-coupled rings: 57 dB for 1 GHz bandwidth, or 117 dB · $Hz^{2/3}$.

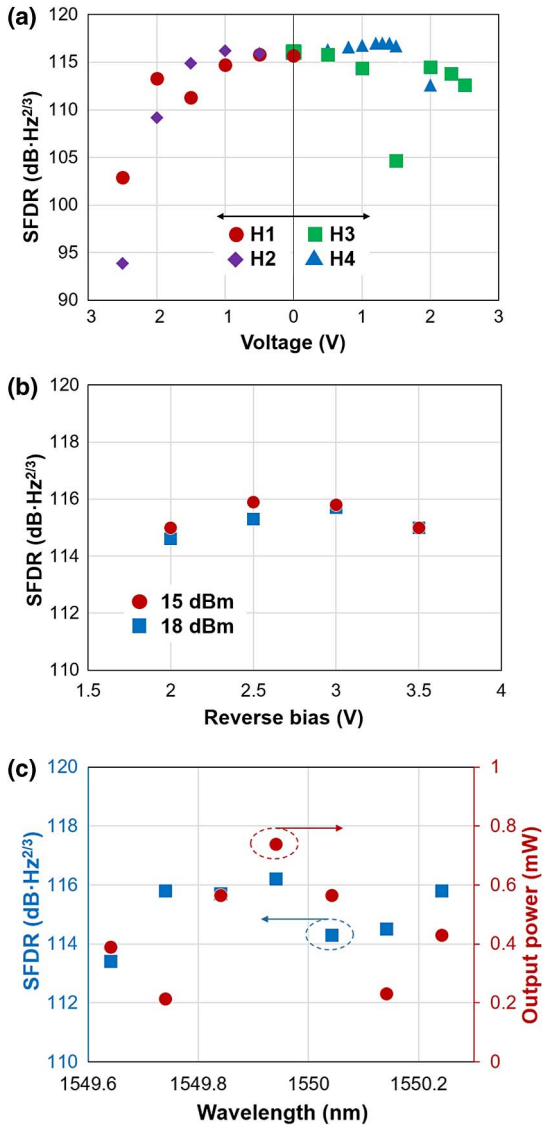

Fig. 5. SFDR measurements of strong-coupled heterogeneous RAMZI modulator for (a) changing the voltage in one of the heaters, H1, H2, H3, or H4 (with all others = 0 V) (modulator bias = –3 V, input power = 18 dBm); (b) changing modulator bias voltage with input power of 15 and 18 dBm, with the voltage in H1 = H2 = H3 = H4 = 0 V; and (c) changing laser wavelength with corresponding output power, with the voltage in heaters H1 = H3 = H4 = 0 V, H2 = 1 V and input power = 18 dBm.

spectrum, as shown in Fig. 5(c). The central point with an SFDR peaked just above 116 dB · $Hz^{2/3}$ shows the wavelength where all other measurements were taken, i.e., centered between two dips of the transmission spectrum. In this figure heater H2 was set to 1 V, while the other heaters were 0 V. A high SFDR value is found versus wavelength across a full FSR from the rings in the RAMZI structure. From a peak value at the center wavelength (1549.941 nm) of 116.2 dB · $Hz^{2/3}$, it drops to a worst-case value of 113.4 dB · $Hz^{2/3}$, still higher than the best result from an MZI style modulator, either a heterogeneous MZI or a standard $LiNbO_3$ MZI modulator. This indicates that the device could be operated at any wavelength and still provide an SFDR of larger than 113 dB · $Hz^{2/3}$, whereas centering the wavelength within the ring FSR provides the highest SFDR. Additionally, the highest SFDR occurs at the condition with the highest modulator output power P_{out}; in this case P_{out} is estimated to be 0.74 mW. The output power P_{out} varies more versus wavelength than the SFDR, due to the dips in the optical transmission spectra of the device, with much lower output power when aligned with these dips.

The RAMZI modulator with weak-coupled rings also shows high linearity. The measurement in Fig. 6 shows an SFDR of 57.5 dB for 1 GHz bandwidth, or 117.5 dB · $Hz^{2/3}$, which is the record-high linearity achieved from a silicon-based modulator. However, this was achieved in a high insertion loss regime, with only 0.07 mW P_{out} (an insertion loss of 20 dB), making this result less practical than the similar SFDR with higher power from the strong-coupled RAMZI modulator.

Figure 7 compares all the SFDR measurements taken for the devices with strong- and weak-coupled rings using the same laser input power of 18 dBm and the same modulator bias of −2.5 V, with various heater bias conditions. A clear trend between SFDR and output power can be seen for each device. For the weak-coupled RAMZI modulator, higher linearity is achieved at low output power. By comparison, the strong-coupled RAMZI has high SFDR over a wide range of power output, with the peak value occurring at an output of about 1 mW. This provides 11 dB of difference in modulator insertion loss between the two designs when operated near maximum SFDR. The fast fall of SFDR with output power and high insertion loss makes the weak-coupled RAMZI less practical, as it requires significant optical gain to achieve the high linearity. Conversely, the strong-coupled RAMZI modulator provided very high SFDR, over 116 dB · $Hz^{2/3}$ over a very wide range of operating parameters and output powers.

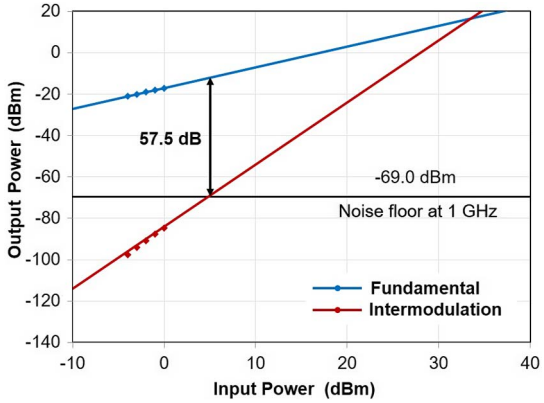

Fig. 6. Measured SFDR of heterogeneous RAMZI modulator with weak-coupled ring design: 57.5 dB for 1 GHz bandwidth, or 117.5 dB · $Hz^{2/3}$.

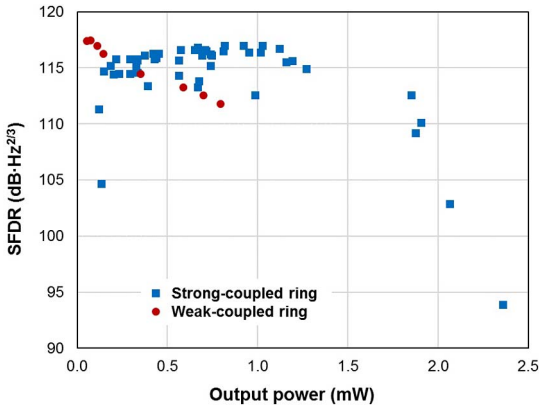

Fig. 7. SFDR measurement of heterogeneous RAMZI modulators with strong- and weak-coupled rings versus modulator output power. The laser input power and the DC bias voltage of the modulator were fixed at 18 dBm and −2.5 V, respectively.

4. SUMMARY

This work demonstrates an ultralinear integrated modulator on silicon using a heterogeneously integrated III–V/Si RAMZI modulator design, achieving a maximum SFDR of 117 dB · $Hz^{2/3}$ for the strong-coupled design, and 117.5 dB · $Hz^{2/3}$ for the weak-coupled design. The strong-coupled heterogeneous RAMZI device had much lower loss at the optimum SFDR bias, and therefore is the most practical for use in system applications. Compared to the standard (i.e., "ringless") heterogeneous MZI [14], the coupled-ring resonant structures of the RAMZI design provide extra tuning degrees of freedom. The positive nonlinearity of the ring phase characteristics is used to efficiently compensate the negative nonlinearity of the MZI transfer response. The RAMZI design achieves SFDR results better than can be achieved with a heterogeneous MZI modulator or a commercial $LiNbO_3$ MZI modulator. This heterogeneous RAMZI modulator provides an ultralinear integrated modulator for the silicon photonics platform, supporting high dynamic range analog optical systems, and integration with other components to form complex RF photonic PICs.

Funding. Morton Photonics and the Defense Advanced Research Projects Agency (DARPA) STTR Program (W91CRB-10-C-0099); Morton Photonics and the Air Force Research Laboratory (AFRL) SBIR Program (FA8650-15-C-1863).

Acknowledgment. The authors thank the nano-fabrication facility at UC Santa Barbara, and Shangjian Zhang, Michael L. Davenport, Sudharsanan Srinivasan, and Geza Kurczveil for useful discussions.

REFERENCES

1. G. C. Valley, "Photonic analog-to-digital converters," Opt. Express **15**, 1955–1982 (2007).

2. W. S. C. Chang, *RF Photonic Technology in Optical Fiber Links* (Cambridge University, 2002), Chap. 4.
3. P. Dong, L. Chen, and Y.-K. Chen, "High-speed low-voltage single-drive push-pull silicon Mach–Zehnder modulators," Opt. Express **20**, 6163–6169 (2012).
4. H. Yi, Q. Long, W. Tan, L. Li, X. Wang, and Z. Zhou, "Demonstration of low power penalty of silicon Mach–Zehnder modulator in long-haul transmission," Opt. Express **20**, 27562–27568 (2012).
5. G. V. Treyz, P. G. May, and J.-M. Halbout, "Silicon Mach–Zehnder waveguide interferometers based on the plasma dispersion effect," Appl. Phys. Lett. **59**, 771–773 (1991).
6. Q. Xu, B. Schmidt, S. Pradhan, and M. Lipson, "Micrometre-scale silicon electro-optic modulator," Nature **435**, 325–327 (2005).
7. M. Streshinsky, A. Ayazi, Z. Xuan, A. E.-J. Lim, G.-Q. Lo, T. Baehr-Jones, and M. Hochberg, "Highly linear silicon traveling wave Mach–Zehnder carrier depletion modulator based on differential drive," Opt. Express **21**, 3818–3825 (2013).
8. C. H. Cox III, E. I. Ackerman, G. E. Betts, and J. L. Prince, "Limits on the performance of RF-over-fiber links and their impact on device design," IEEE Trans. Microwave Theory Tech. **54**, 906–920 (2006).
9. R.-J. Essiambre, P. J. Winzer, X. Wang, W. Lee, C. A. White, and E. C. Burrows, "Electronic predistortion and fiber nonlinearity," IEEE Photon. Technol. Lett. **18**, 1804–1806 (2006).
10. C. Weber, C.-A. Bunge, and K. Petermann, "Fiber nonlinearities in systems using electronic predistortion of dispersion at 10 and 40 Gbit/s," J. Lightwave Technol. **27**, 3654–3661 (2009).
11. X. Xie, J. B. Khurgin, J. Kang, and F.-S. Chow, "Linearized Mach–Zehnder intensity modulator," IEEE Photon. Technol. Lett. **15**, 531–533 (2003).
12. J. Cardenas, P. A. Morton, J. B. Khurgin, A. Griffith, C. B. Poitras, K. Preston, and M. Lipson, "Linearized silicon modulator based on a ring assisted Mach–Zehnder interferometer," Opt. Express **21**, 22549–22557 (2013).
13. L. Chen, J. Chen, J. Nagy, and R. M. Reano, "Highly linear ring modulator from hybrid silicon and lithium niobate," Opt. Express **23**, 13255–13264 (2015).
14. C. Zhang, P. A. Morton, J. B. Khurgin, J. D. Peters, and J. E. Bowers, "Highly linear heterogeneous-integrated Mach–Zehnder interferometer modulators on Si," Opt. Express **24**, 19040–19047 (2016).
15. H.-W. Chen, Y.-H. Kuo, and J. E. Bowers, "A hybrid silicon-AlGaInAs phase modulator," IEEE Photon. Technol. Lett. **20**, 1920–1922 (2008).
16. Y. Zhou, L. Zhou, F. Su, J. Xie, H. Zhu, X. Li, and J. Chen, "Linearity measurement of a silicon single-drive push-pull Mach–Zehnder modulator," in *Conference on Lasers and Electro-Optics* (Optical Society of America, 2015), paper SW3N.6.